

Nickel(II) ion-intercalated MXene membranes for enhanced H₂/CO₂ separation

Yiyi Fan^{1*}, Jinyong Li^{1*}, Saidi Wang¹, Xiuxia Meng (✉)¹, Yun Jin¹, Naitao Yang¹, Bo Meng¹,
Jiaquan Li², Shaomin Liu (✉)^{2,3}

¹ School of Chemical Engineering, Shandong University of Technology, Zibo 255049, China

² Department of Chemical Engineering, Curtin University, Perth, WA 6845, Australia

³ College of Chemical Engineering, Beijing University of Chemical Technology, Beijing 100029, China

© Higher Education Press 2020

Abstract Hydrogen fuel has been embraced as a potential long-term solution to the growing demand for clean energy. A membrane-assisted separation is promising in producing high-purity H₂. Molecular sieving membranes (MSMs) are endowed with high gas selectivity and permeability because their well-defined micropores can facilitate molecular exclusion, diffusion, and adsorption. In this work, MXene nanosheets intercalated with Ni²⁺ were assembled to form an MSM supported on Al₂O₃ hollow fiber via a vacuum-assisted filtration and drying process. The prepared membranes showed excellent H₂/CO₂ mixture separation performance at room temperature. Separation factor reached 615 with a hydrogen permeance of $8.35 \times 10^{-8} \text{ mol} \cdot \text{m}^{-2} \cdot \text{s}^{-1} \cdot \text{Pa}^{-1}$. Compared with the original Ti₃C₂T_x/Al₂O₃ hollow fiber membranes, the permeation of hydrogen through the Ni²⁺-Ti₃C₂T_x/Al₂O₃ membrane was considerably increased, stemming from the strong interaction between the negatively charged MXene nanosheets and Ni²⁺. The interlayer spacing of MSMs was tuned by Ni²⁺. During 200-hour testing, the resultant membrane maintained an excellent gas separation without any substantial performance decline. Our results indicate that the Ni²⁺ tailored Ti₃C₂T_x/Al₂O₃ hollow fiber membranes can inspire promising industrial applications.

Keywords MXene, H₂/CO₂ separation, nickel ions, hollow fiber

1 Introduction

The separation of gas mixtures is crucial in various industrial processes [1]. Traditional techniques such as pressure swing adsorption and cryogenics suffer from an immense energy consumption [2]. By contrast, membrane separation systems are energy efficient and environmentally friendly. They are also easy to set up and operate [3–6]. However, one of the greatest challenges for membrane separation is low selectivity, permeance, and stability. Based on the principle of solution-diffusion, polymer membranes generally suffer from a trade-off of gas permeance and selectivity restricted by Robeson upper bounds [7,8]. Molecular sieving membranes (MSMs) are endowed with a high selectivity and permeability due to the well-defined microporous structure facilitating molecular size exclusion, diffusion, and preferable adsorption; thus, they have been widely studied and reported [9–12]. However, the prohibitive cost of synthesis and the difficulty in achieving desired selectivity during scaling up makes MSMs incapable of industrial applications. Recently, 2D materials, such as zeolite [13–15], metal-organic framework (MOF) [16–18], graphene [19], and graphene oxide [9,20–22], have become very attractive for assembling composite MSMs. Numerous studies have reported their applications in the fields of water purification, oil/water separation, and gas separation [20–22].

Compared with other 2D membrane materials, MXene with the general formula M_{n+1}X_nT_x has shown good dispersion in an aqueous solution resulting from abundant terminating groups (–F, –OH, and –O–) on its surfaces and edges [23–25]. The hydrophilic surface is beneficial for assembling the separation membrane by vacuum filtration. Moreover, MXene exhibits excellent high-temperature tolerance; therefore, it is applicable to the chemical process industry [26,27]. However, very few reports used 2D

Received May 20, 2020; accepted July 10, 2020

E-mails: mengxiux@sdut.edu.cn (Meng X);

shaomin.liu@curtin.edu.au (Liu S)

*These authors contributed equally to this work

MXene nanosheets to assemble membranes for molecule/ion separation [28]. In 2015, Wang et al. [29] first constructed 2D MXene nanosheets on commercial polyvinylidene fluoride supports for selective sieving cations based on hydration radius and charge of the ions. Wang's group [30] prepared MXene membranes by filtering Ti₃C₂T_x nanosheets on anodic aluminum oxide membrane, showing an excellent water permeance (more than 1000 L·m⁻²·h⁻¹·bar⁻¹) and a favorable rejection rate for large molecules. Subsequently, they [31,32] further optimized the regular subnanometer channels of MXene membrane for application in molecular sieving for gas separation. Jin's group [33] developed a Ti₃C₂T_x nanofilm with a thickness down to 20 nm, exhibiting excellent permeability and selectivity for hydrogen. MXene membranes have a preferential selectivity for CO₂ permeation from its mixture by a clever tuning on the interlayer spacing using small inorganic or polymeric molecules capturing CO₂. These studies show that tailoring the spacing of adjacent MXene nanosheets is a prerequisite to match selective permeation along its regular and tortuous 2D channels of laminar MXene membrane. Therefore, many strategies have been applied to tailor the spacing through sandwiching appropriately sized fillers between 2D nanosheets [34–36]. Among them, cationic intercalation is a valid method to tune interlayer spacing. Two functions are available for cationic intercalation into MXene nanosheets: 1) Electrostatic repulsion is weakened between MXene nanosheets with a negative charge, resulting in increasing regularity of the membrane instead of conglomeration. 2) Interlayer spacing of laminar membrane is tuned by promoting a strong interaction between neighboring MXene nanosheets from cationic intercalation [37]. The MXene-based composite membrane modified by metal cation has been applied in electro-

chemical device and has shown high performance [38,39]. However, no reports have been made on cation-modified MXene-based MSMs for gas separation.

Compared with pallet supports, a ceramic hollow fiber with a much higher area/volume ratio is more applicable to minimize the volume of membrane separation system, resulting in reduced investment and operational cost [40,41]. Herein, we prepare a cation Ni²⁺-intercalated MXene membrane on an alumina hollow fiber support (Ni²⁺-Ti₃C₂T_x/Al₂O₃), as shown Fig. 1. Electrostatic repulsion between the two adjacent nanosheets is weakened due to the intercalation of nickel ions, leading to increasing mutual interaction, by which the nanochannel of the MXene membrane becomes more well-organized. Further, the expanding interlayer spacing leads to a high permeance of hydrogen. Molecular sieving channels in Ni²⁺-Ti₃C₂T_x/Al₂O₃ hollow fiber membranes show high H₂ selectivity from its mixture, transcending the state-of-the-art membrane.

2 Experimental

2.1 Preparation of composite membrane

MXene powder was synthesized by a mild etching method. Briefly, 1 g of LiF (purchased from Aladdin) and 0.2 g of NiCl₂·6H₂O (purchased from Aladdin) were dissolved in 20 mL of HCl (6 mol·L⁻¹) solution in a Teflon beaker. Subsequently, 1 g Ti₃AlC₂ powder (purchased from Laizhou Kai Ceramic Materials) was slowly added to the solution with magnetic stirring at 45 °C for 24 h. A clay-like sediment was obtained and washed with deionized water until the pH of supernatant > 6. The sediment was dispersed in 150 mL of deionized water with magnetic

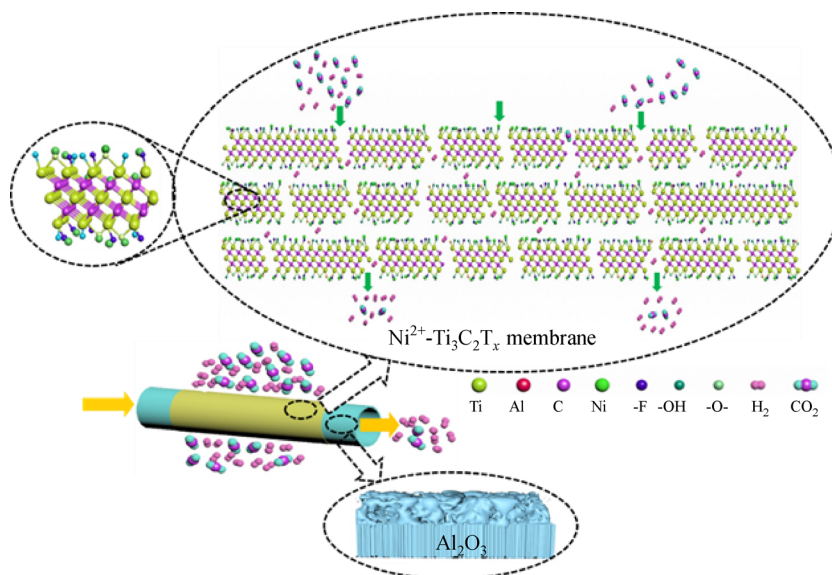


Fig. 1 Schematic diagram of hydrogen and CO₂ mixture separation by Ni²⁺-Ti₃C₂T_x/Al₂O₃ hollow fiber membrane.

stirring and sonication for 40 min to prepare MXene flakes. The stable Ni^{2+} - $\text{Ti}_3\text{C}_2\text{T}_x$ colloidal solution was obtained after centrifugation at $5000 \text{ r}\cdot\text{min}^{-1}$ for 30 min. Vacuum-assisted filtration was applied to assemble Ni^{2+} - $\text{Ti}_3\text{C}_2\text{T}_x$ laminates on the surface of Al_2O_3 hollow fiber as reported previously [42]. Then, the obtained Ni^{2+} - $\text{Ti}_3\text{C}_2\text{T}_x/\text{Al}_2\text{O}_3$ membranes were prepared by vacuum drying at 120°C for 12 h (Fig. 2). $\text{Ti}_3\text{C}_2\text{T}_x/\text{Al}_2\text{O}_3$ membrane was prepared using $\text{Ti}_3\text{C}_2\text{T}_x$ nanosheets, and the subsequent treatment conditions were maintained similarly as those for preparing Ni^{2+} - $\text{Ti}_3\text{C}_2\text{T}_x/\text{Al}_2\text{O}_3$ membranes.

2.2 Gas permeance of supported MXene membranes

Single-gas permeation was performed at room temperature to determine the gas separation performance of Ni^{2+} - $\text{Ti}_3\text{C}_2\text{T}_x/\text{Al}_2\text{O}_3$ membrane. A bubble flow meter was employed to detect the flow rate of permeated single gas, and permeance was calculated in terms of Eq. (1):

$$P_i^* = \frac{N_i}{(p_1 - p_2)}, \quad (1)$$

where P_i^* is the single-gas permeance ($\text{mol}\cdot\text{m}^{-2}\cdot\text{s}^{-1}\cdot\text{Pa}^{-1}$), N_i is the molar flux of gas (i) ($\text{mol}\cdot\text{m}^{-2}\cdot\text{s}^{-1}$), and p_1 or p_2 are the pressures (Pa) at the feed side or permeate side. The ideal selectivity (single-component selectivity) between gas components i and j of the gas pair can be calculated by Eq. (2).

$$S_{ij} = \frac{P_i^*}{P_j^*}. \quad (2)$$

In the case of gas mixtures, permeance and mixture selectivity or separation factor are defined as follows:

$$P_i^* = \frac{N_i}{(p_{i1} - p_{i2})}, \quad (3)$$

$$a_{ij} = \frac{y_{i2}/y_{j2}}{y_{i1}/y_{j1}}, \quad (4)$$

where p_{i1} and p_{i2} are the partial pressures (Pa) of the component at the feed or permeated side; $y_{i1}, y_{i2}, y_{j1}, y_{j2}$ are the volumetric fractions of component i or j in the feed or permeated side gas mixtures. Subscripts “1” and “2” refer to the feed side and permeate side, respectively.

The performance of the composite membranes was determined in a home-made device, as displayed in Fig. 3. Feed gas consisted of H_2 and other gases ($\text{CO}_2, \text{N}_2,$ and CH_4) with a volume ratio of 1:1, and flow rate was $60 \text{ mL}\cdot\text{min}^{-1}$. Synchronously, argon was used as sweep gas with a flow rate of $60 \text{ mL}\cdot\text{min}^{-1}$ at standard pressure. Gas composition on the sweep side was measured using an online gas chromatograph (7890B, Agilent) with thermal conductivity detector.

2.3 Characterization of MXene nanosheets and membranes

The microstructure of MXene films and composite membranes was characterized using field emission scanning electron microscopy (SEM, FEI Apreo S, Thermo-fisher). Images were obtained using transmission electron microscopy (TEM, Titan) with an acceleration voltage of 200 kV. The crystal structure of $\text{Ti}_3\text{C}_2\text{T}_x$ powder power and composite membranes were determined using powder X-ray diffraction (XRD, Bruker D8 Advance, Germany) using $\text{Cu-K}\alpha$ radiation ($\lambda = 0.15404 \text{ nm}$) in the range of 5° – 80° with a step size of 0.02° and a scan rate of $2^\circ\cdot\text{min}^{-1}$. Functional groups of MXene membranes were character-

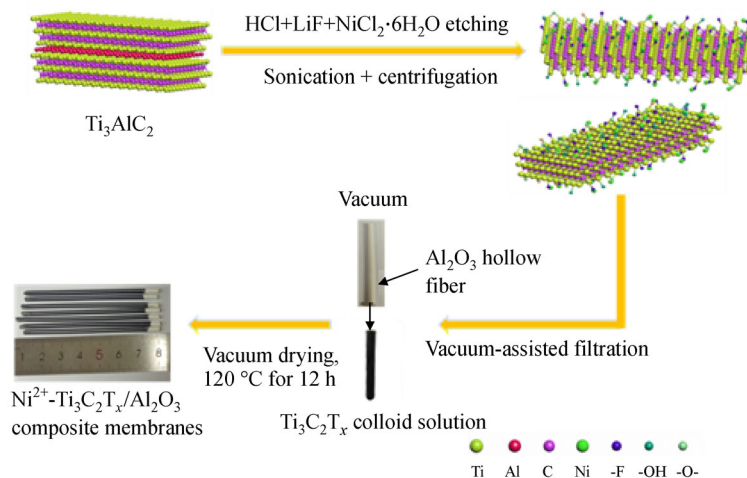


Fig. 2 Preparation of Al_2O_3 supported Ni^{2+} - $\text{Ti}_3\text{C}_2\text{T}_x$ membranes.

ized by Fourier transform infrared spectrometer (FTIR, Nicolet 5700, USA). The morphology of Ti₃C₂T_x films after nickel ion modification was characterized using an atomic force microscope (AFM, XE-100, Korea).

3 Results and discussion

3.1 Morphology of MXene films after Ni²⁺ modification

Many advanced properties of 2D layered materials like MXene are associated with the presence of functional groups. Similarly, the nanosheets of MXene with proper functional groups are crucial for preparing high-quality 2D membranes. The mixed solution of (LiF) and HCL was selected instead of hydrogen fluoride as the etchant (HF) to prepare defect-free MXene nanosheets under a mild condition. Ni²⁺-Ti₃C₂T_x nanosheets were obtained after selectively etching Al from the corresponding MAX (Ti₃AlC₂) precursor by using etching solution containing

Ni²⁺ followed by ultrasonication and centrifugation. The Ti₃AlC₂ sample clearly has a layered structure which is firmly held together, as shown in Fig. S1(a) (cf. Electronic Supplementary Material, ESM). The accordion-like structure of Ni²⁺-Ti₃C₂T_x powder indicates the successful removal of Al atom from the MAX phase of Ti₃AlC₂, as shown in Fig. 4(a) and Fig. S1(b). The Tyndall scattering effect was clearly observed after sonication and centrifugation, as shown in Fig. 4(b) inset, confirming that a stable colloidal solution was prepared. SEM images of the exfoliated MXene nanosheets on anodic aluminum oxide substrate in Fig. 4(b) show that the exfoliated MXene nanosheets were very thin and nearly transparent to the electron beams. Ti, C, O, F, and Ni were uniformly distributed, as shown in energy dispersive X-ray spectroscopy images of the selected area in Fig. S2 (cf. ESM), which suggests that nickel ions were successfully intercalated between MXene layers. TEM, high-resolution TEM, and selected area electron diffraction (SAED) of nanosheets in Fig. 4(c), and Supplementary Figs. 1(c,d)

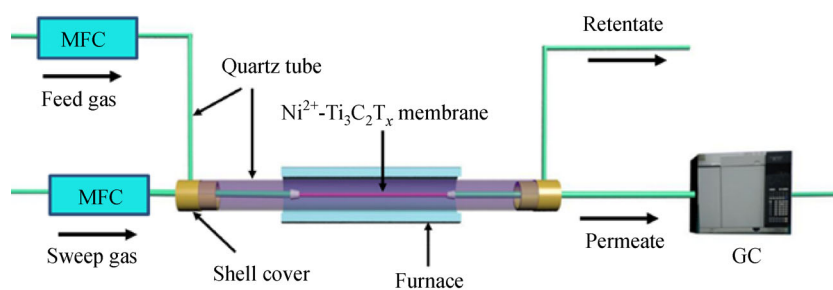


Fig. 3 Diagram of the home-made device for mixture gas permeability test of composite membranes.

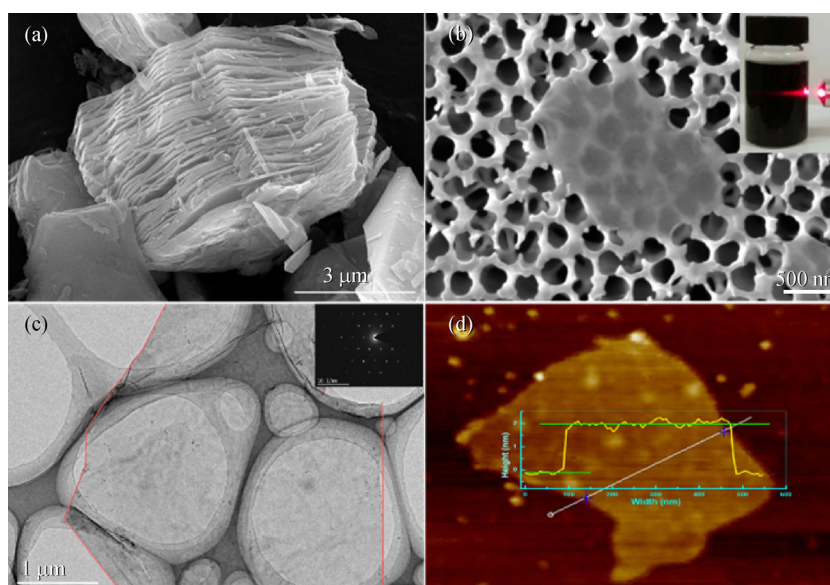


Fig. 4 (a) SEM images of synthesized Ti₃C₂T_x powder, (b) Ni²⁺-Ti₃C₂T_x nanosheets (inset showing the Tyndall scattering effect of Ni²⁺-Ti₃C₂T_x colloidal solution), and (c) TEM and (d) AFM images of Ni²⁺-Ti₃C₂T_x nanosheets.

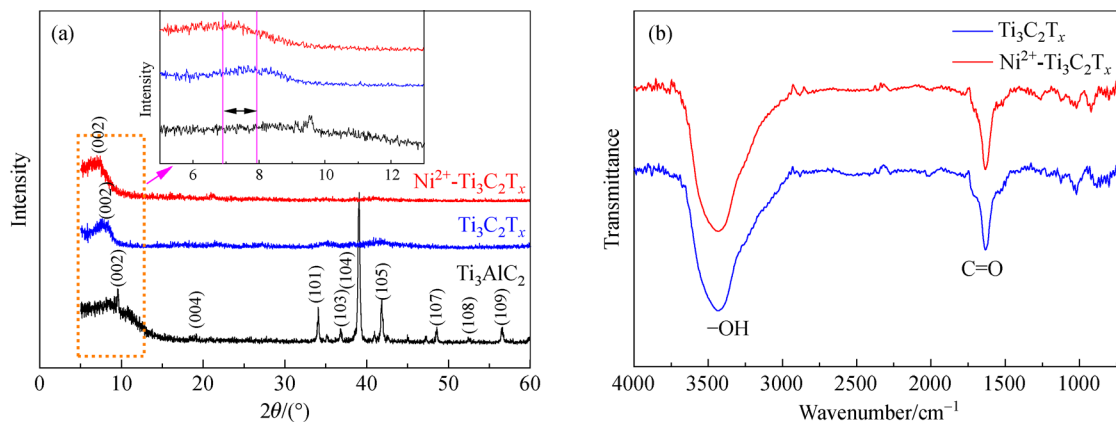


Fig. 5 (a) XRD patterns of Ti_3AlC_2 , $\text{Ti}_3\text{C}_2\text{T}_x$, and $\text{Ni}^{2+}\text{-Ti}_3\text{C}_2\text{T}_x$ power with inset of the magnified XRD pattern at low Bragg angles; (b) FTIR spectra of MXene and nickel ion functionalized MXene.

clearly depict the high crystallinity of synthesized 2D $\text{Ni}^{2+}\text{-Ti}_3\text{C}_2\text{T}_x$ sheets without apparent nanometer-scale defects. The AFM image of $\text{Ni}^{2+}\text{-Ti}_3\text{C}_2\text{T}_x$ nanosheet had a thickness of ~ 2 nm, as shown in Fig. 4(d), demonstrating that a nanosheet of about two layers of MXene was obtained after sonication and centrifugation.

As shown in Fig. 5(a), the crystallinity of the synthesized MXene nanocrystals and the MAX power was further studied by XRD. The diffraction peak for the (104) planes of Ti_3AlC_2 located at 39° disappeared in the XRD pattern of $\text{Ti}_3\text{C}_2\text{T}_x$, meaning that the Al layers were removed by etching. This finding is consistent with previous literature results [43,44]. Additionally, the (002) peak shifted toward a lower 2θ value from 9.52° to 7.74° , which is evidenced more clearly by the magnified part of the XRD patterns at lower diffraction angles. The calculated interlayer spacing of the MXene ($\text{Ti}_3\text{C}_2\text{T}_x$) was about 11.40 \AA , which was enlarged to 12.68 \AA ($\text{Ni}^{2+}\text{-Ti}_3\text{C}_2\text{T}_x$) after Ni^{2+} intercalation. This observation indicates a successful intercalation of Ni^{2+} into the $\text{Ti}_3\text{C}_2\text{T}_x$ flakes. In Fig. 5(b), the stretching vibration at 3434 and 1633 cm^{-1} represented the functional groups of -OH and C=O, which demonstrate the -OH and C=O terminal groups on the MXene surface. Compared with the peak strength and position of $\text{Ti}_3\text{C}_2\text{T}_x$ power, $\text{Ni}^{2+}\text{-Ti}_3\text{C}_2\text{T}_x$ did not change. This finding indicates that a minor Ni^{2+} intercalation during etching had no effect on surface properties of MXene nanosheets.

3.2 Gas separation behavior of supported MXene membranes

We assembled Ni^{2+} -modified nanosheets on Al_2O_3 hollow fiber membrane using a vacuum-assisted filtration method and drying process to verify our hypothesis that nickel ions can tune the gas transport behavior of the MXene membrane. In this work, the porous alumina hollow fiber was used as a substrate to deposit MXene nanosheets. As

shown in Fig. 6(a), the Al_2O_3 hollow fiber had an asymmetric porous cross-section structure and a porous surface, which was tailored by controlling the preparation parameters in the phase inversion process. After the successful preparation of MXene membranes, the white outer surface of Al_2O_3 hollow fiber became bright black (Fig. 2). The cross-sectional SEM image of the $\text{Ni}^{2+}\text{-Ti}_3\text{C}_2\text{T}_x/\text{Al}_2\text{O}_3$ membrane was present in Fig. 6(b), indicating that the MXene membrane was firmly adhered on the porous substrate. The thickness of the MXene membrane was about $2.7\text{ }\mu\text{m}$, which showed a morphology similar to other 2D material membranes prepared for gas separation [26,33,42]. A regular layer-by-layer stacked structure of the composite membrane can be clearly observed in Fig. 6(d). The regularity of nanochannels was also supported by the sharp peak (002) in XRD patterns of the membrane (Fig. S4, cf. ESM). The surface of the composite membrane stacked by $\text{Ni}^{2+}\text{-Ti}_3\text{C}_2\text{T}_x$ nanosheets showed a typical wave-like structure similar to the graphene oxide membrane, as shown in Fig. 6(c) [22,45]. No evident defects and pinholes were seen from the membrane surface. The dense, continuous lamellar nanochannels can be used for gas separation, as shown in Fig. 6(d).

The gas separation performance of the composite membranes was evaluated in a home-made device. The separation of various gas mixtures containing equimolar hydrogen and other gases including H_2/CO_2 , H_2/N_2 and H_2/CH_4 was studied. Table 1 shows that the separation factor and the permeation of hydrogen through the $\text{Ni}^{2+}\text{-Ti}_3\text{C}_2\text{T}_x/\text{Al}_2\text{O}_3$ membrane was considerably increased compared with the $\text{Ti}_3\text{C}_2\text{T}_x/\text{Al}_2\text{O}_3$ membrane (Fig. S3, cf. ESM). Separation factors for H_2/CO_2 , H_2/N_2 , and H_2/CH_4 pairs were 615, 154.48 and 147.27, respectively, with corresponding hydrogen permeances of 8.35 , 8.79 , and $9.52 \times 10^{-8}\text{ mol}\cdot\text{m}^{-2}\cdot\text{s}^{-1}\cdot\text{Pa}^{-1}$, respectively. The higher separation factor of $\text{Ni}^{2+}\text{-Ti}_3\text{C}_2\text{T}_x/\text{Al}_2\text{O}_3$ membrane was due to the positively charged cation

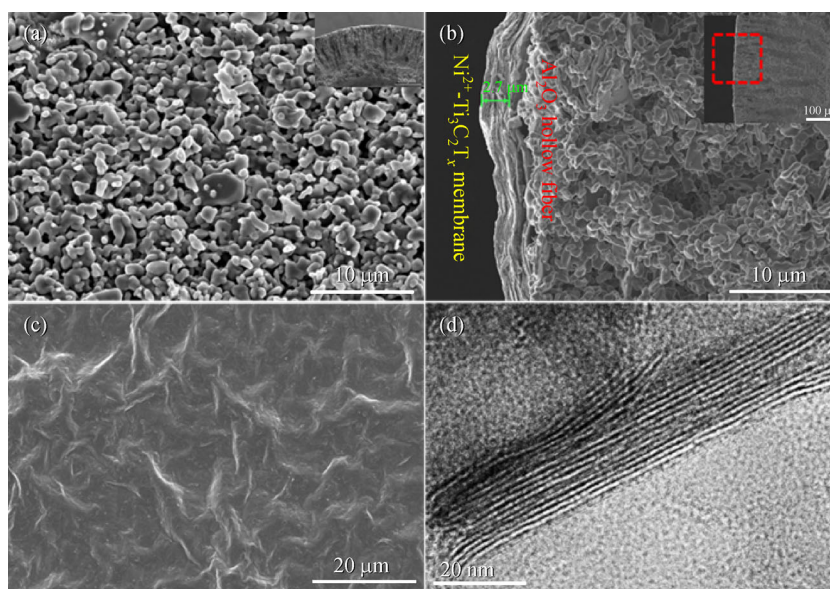


Fig. 6 SEM images of the outer surface (a) of the Al₂O₃ hollow fiber support (before deposition of MXene) with the inset showing the cross-section, the high magnification of the Ni²⁺-Ti₃C₂T_x/Al₂O₃ membrane, (b) showing the thickness around 2.7 μm with the inset showing the lower magnification, (c) the surface of the Ni²⁺-Ti₃C₂T_x/Al₂O₃ membrane, and (d) the TEM image of the Ni²⁺-Ti₃C₂T_x/Al₂O₃ membrane.

Table 1 Separation performance of MXene/Al₂O₃ and Ni²⁺-Ti₃C₂T_x/Al₂O₃ membrane

Mixed gas ^{a)}	Knudsen constant	MXene/Al ₂ O ₃		Ni ²⁺ -Ti ₃ C ₂ T _x /Al ₂ O ₃	
		Separation factor	Permeability/(10 ⁻⁸ mol·m ⁻² ·s ⁻¹ ·Pa ⁻¹)	Separation factor	Permeability/(10 ⁻⁸ mol·m ⁻² ·s ⁻¹ ·Pa ⁻¹)
H ₂ /CO ₂	4.69	215.25	5.29	615	8.35
H ₂ /N ₂	3.74	99.13	6.76	154.48	8.79
H ₂ /CH ₄	2.82	94.35	7.11	147.27	9.52

a) The molar ratio of mixed gases was 1:1.

incorporated into Ti₃C₂T_x which weakened the electrostatic repulsion, resulting in the increase of the interaction between the adjacent MXene nanosheets [46]. It favored membrane formation using laminar MXene nanosheets with a more regular structure, as shown in Fig. 6(d) [47]. The SAED patterns (Fig. S5, cf. ESM) show that Ni²⁺ was evenly distributed in the selected region, indicating that the interlayer spacing of composite membrane was tuned by Ni²⁺. Therefore, the permeation and separation factors of Ni²⁺-Ti₃C₂T_x membrane increased compared with the MXene membrane.

Single-gas permeation was carried out using a series of single gases with different kinetic diameters at room temperature to explore the molecular sieving properties of the Ni²⁺-Ti₃C₂T_x/Al₂O₃ membrane further. As shown in Fig. 7(a), the permeability of small gas molecules (He or H₂) was much higher than those of gas molecules with large kinetic diameters such as CO₂, N₂, and CH₄. Permeances declined in the order of H₂ (0.289 nm), He (0.26 nm), CH₄ (0.384 nm), N₂ (0.364 nm), CO₂

(0.33 nm), which is consistent with other researchers [9,48]. The higher permeance for the sphere CH₄ molecules than the rod-shape N₂ molecules was attributed to the molecular shape; the sphere molecules might be easier to permeate through nanochannels of Ni²⁺-Ti₃C₂T_x membranes due to less steric hindrance [9,42,49]. The less permeable CO₂ was due to not only the rod-like shape of the molecule but also the extremely strong quadrupole moment than N₂ and CH₄. The ideal selectivity of H₂/CO₂ was about 750, far exceeding the Knudsen selectivity of 4.7. The ideal selectivities of other gas pairs, i.e., H₂/N₂, H₂/CH₄, were 430 and 240, respectively. This superior selectivity was much higher than that of other 2D separation membranes [50–52]. This finding presents potential applications of the composite membranes to separation of H₂ from a mixture gas containing hydrogen. Figure 7(b) displays that the permeance of H₂ and CO₂ for Ni²⁺-Ti₃C₂T_x/Al₂O₃ membrane increased with increasing the temperature from 25 °C to 120 °C. The separation factor of H₂/CO₂ decreased from 650 at 25 °C to 186 at

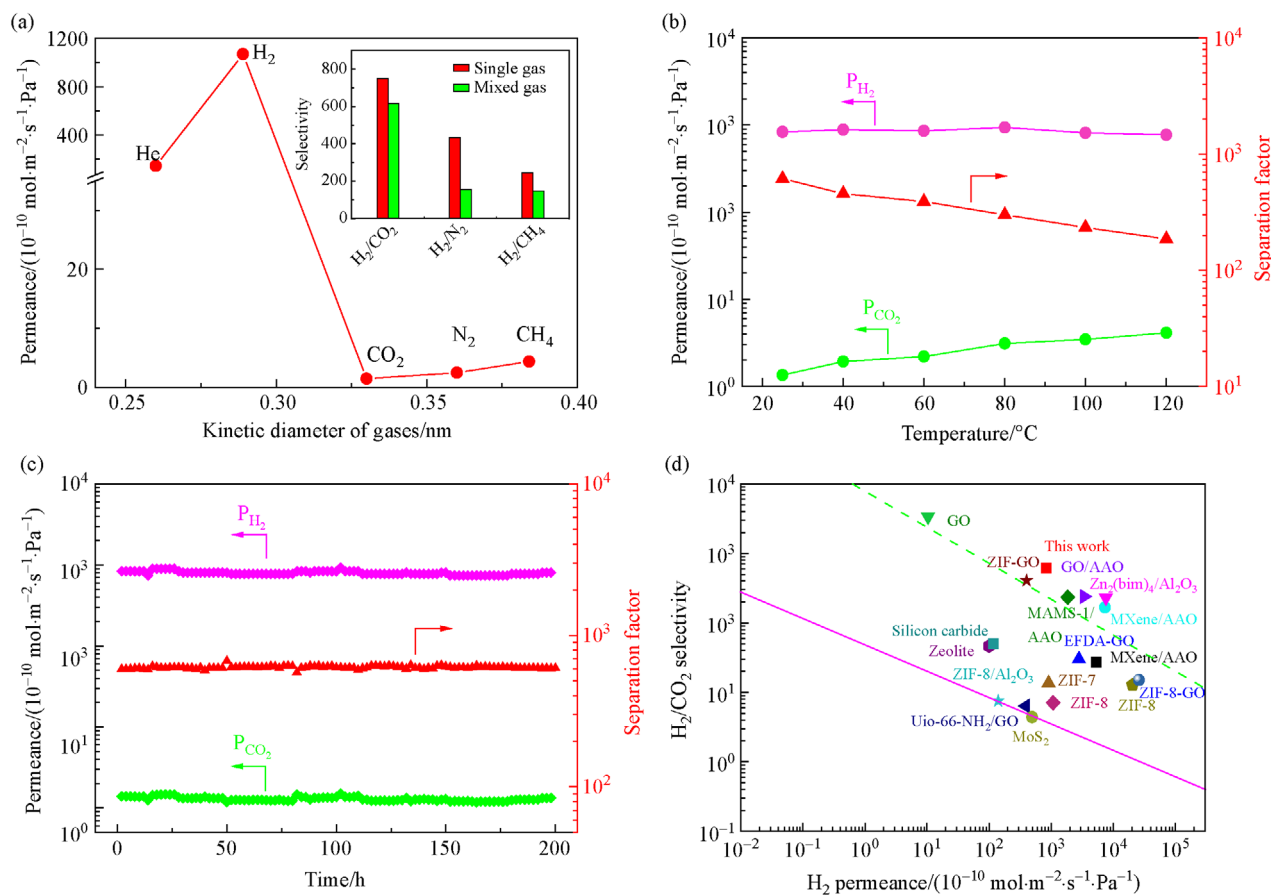


Fig. 7 (a) Single-gas permeance through the supported Ni^{2+} - $\text{Ti}_3\text{C}_2\text{T}_x$ membrane at room temperature, (b) separation performance of the Ni^{2+} - $\text{Ti}_3\text{C}_2\text{T}_x/\text{Al}_2\text{O}_3$ membrane as a function of temperature in the equimolar mixed-gas H_2/CO_2 , (c) long-term separation of equimolar mixed-gas H_2/CO_2 through a Ni^{2+} - $\text{Ti}_3\text{C}_2\text{T}_x/\text{Al}_2\text{O}_3$ membrane at RT, H_2/CO_2 separation performance, and (d) of the $\text{Ti}_3\text{C}_2\text{T}_x/\text{Al}_2\text{O}_3$ membrane compared with state-of-the-art gas separation membranes. The red line indicates the Robeson 2008 upper bound of polymeric membranes for H_2/CO_2 separation, and the dashed green line represents the 2017 upper bound of the best current membranes for H_2/CO_2 separation. More information of the data is given in Table S1 (cf. ESM).

120 $^\circ\text{C}$ because the permeance of CO_2 increased more rapidly than H_2 with increasing temperature. A long-term permeation measurement was carried out for H_2/CO_2 mixture at the operation temperature of 25 $^\circ\text{C}$ to verify the stable separation performance of the composite membrane. As shown in Fig. 7(c), the composite membrane maintained an excellent separation performance and no substantial change of the permeance during more than 200-hour long-term operation testing. This result indicates that the Ni^{2+} - $\text{Ti}_3\text{C}_2\text{T}_x/\text{Al}_2\text{O}_3$ membrane was mechanically robust such that no defects were generated under the longtime continuous gas permeation, which is important for dealing with mixtures containing hydrogen in practical industries [22]. Compared with previously reported membranes, the supported Ni^{2+} - $\text{Ti}_3\text{C}_2\text{T}_x$ membrane exhibited a superior H_2 selectivity, which considerably exceeds the latest upper bound of most current membranes, as shown in Fig. 7(d) [9,10,12,17,22,31,33,48,51–59]. The

unprecedented preferential H_2 permeation could be due to the increasing interlayer spacing and capture of CO_2 from the unique cation intercalation between the adjacent $\text{Ti}_3\text{C}_2\text{T}_x$ laminates similar with the metal ion-modified MOFs [60].

4 Conclusions

In summary, a promising cation-intercalated MXene membrane (Ni^{2+} - $\text{Ti}_3\text{C}_2\text{T}_x$) on porous alumina hollow fiber support was prepared using a vacuum-assisted filtration and drying process. The divalent nickel ion intercalation into the MXene membrane effectively enhanced the interaction between nanosheets by reducing the repulsion between adjacent nanosheets. Further, the decreasing stacking behavior and increasing interlayer spacing of Ni^{2+} - $\text{Ti}_3\text{C}_2\text{T}_x$ membranes were precisely tuned

by the Ni²⁺ intercalation. These new properties led to the excellent gas separation of the resultant hollow fiber-supported MXene membrane. At room temperature, the separation factor for H₂/CO₂ mixture reached 615 with a superior hydrogen permeance of 8.35×10^{-8} mol·m⁻²·s⁻¹·Pa⁻¹. In a 200-hour stability test, selectivity and permeation properties were maintained constant without performance decay. These observations indicate that the Ni²⁺ intercalated MXene membrane has a good industrial application prospect.

Acknowledgements This work was financially supported by the National Natural Science Foundation of China (Grant Nos. 21776165, 21878179 and 21978157). Naitao Yang gratefully thanks the support via Natural Science Foundation of Shandong Province (ZR2019MB056). Shaomin Liu acknowledges the financial support provided by the Australian Research Council (DP180103861).

Electronic Supplementary Material Supplementary material is available in the online version of this article at <https://doi.org/10.1007/s11705-020-1990-1> and is accessible for authorized users.

References

- Liu M, Gurr P A, Fu Q, Webley P A, Qiao G G. Two-dimensional nanosheet-based gas separation membranes. *Journal of Materials Chemistry. A, Materials for Energy and Sustainability*, 2018, 6(46): 23169–23196
- Wang J, Zhu J, Zhang Y, Liu J, Van der Bruggen B. Nanoscale tailor-made membranes for precise and rapid molecular sieve separation. *Nanoscale*, 2017, 9(9): 2942–2957
- Sunarjo J, Hashim S S, Lin Y S, Liu S. Membranes for helium recovery: an overview on the context, materials and future directions. *Separation and Purification Technology*, 2017, 176: 335–383
- Nezhad F A, Han N, Jin Y, Shen Z, Wang Y, Yang N, Liu S. Experimental and theoretical exploration of gas permeation mechanism through 2D graphene (not graphene oxides) membranes. *Journal of Membrane Science*, 2020, 601: 117883
- Gin D L, Noble R D. Designing the next generation of chemical separation membranes. *Science*, 2011, 332(6030): 674–676
- Park H B, Kamcev J, Robeson L M, Elimelech M, Freeman B D. Maximizing the right stuff: the trade-off between membrane permeability and selectivity. *Science*, 2017, 356(6343): eaab0530
- Bernardo P, Drioli E, Golemme G. Membrane gas separation: a review/state of the art. *Industrial & Engineering Chemistry Research*, 2009, 48(10): 4638–4663
- Lau C H, Li P, Li F, Chung T S, Paul D R. Reverse-selective polymeric membranes for gas separations. *Progress in Polymer Science*, 2013, 38(5): 740–766
- Li H, Song Z, Zhang X, Huang Y, Li S, Mao Y, Ploehn H J, Bao Y, Yu M. Ultrathin, molecular-sieving graphene oxide membranes for selective hydrogen separation. *Science*, 2013, 342(6154): 95–98
- Battersby S, Tasaki T, Smart S, Ladewig B, Liu S, Duke M C, Rudolph V, Diniz da Costa J C. Performance of cobalt silica membranes in gas mixture separation. *Journal of Membrane Science*, 2009, 329(1-2): 91–98
- Liu Y, Wang N, Cao Z, Caro J. Molecular sieving through interlayer galleries. *Journal of Materials Chemistry. A, Materials for Energy and Sustainability*, 2014, 2(5): 1235–1238
- Wang X, Chi C, Zhang K, Qian Y, Gupta K M, Kang Z, Jiang J, Zhao D. Reversed thermo-switchable molecular sieving membranes composed of two-dimensional metal-organic nanosheets for gas separation. *Nature Communications*, 2017, 8(1): 14460–14469
- Jeong H K, Nair S, Vogt T, Dickinson L C, Tsapatsis M. A highly crystalline layered silicate with three-dimensionally microporous layers. *Nature Materials*, 2003, 2(1): 53–58
- Tsapatsis M. 2-Dimensional zeolites. *AIChE Journal*, 2014, 60(7): 2374–2381
- Agrawal K V, Topuz B, Pham T C, Nguyen T H, Sauer N, Rangnekar N, Zhang H, Narasimharao K, Basahel S N, Francis L F, Macosko C W, Al-Thabaiti S, Tsapatsis M, Yoon K B. Oriented MFI membranes by gel-less secondary growth of sub-100 nm MFI-Nanosheet seed layers. *Advanced Materials*, 2015, 27(21): 3243–3249
- Venna S R, Lartey M, Li T, Spore A, Kumar S, Nulwala H B, Luebke D R, Rosi N L, Albenze E. Fabrication of MMMs with improved gas separation properties using externally-functionalized MOF particles. *Journal of Materials Chemistry. A, Materials for Energy and Sustainability*, 2015, 3(9): 5014–5022
- Peng Y, Li Y, Ban Y, Jin H, Jiao W, Liu X, Yang W. Membranes. Metal-organic framework nanosheets as building blocks for molecular sieving membranes. *Science*, 2014, 346(6215): 1356–1359
- Zhao Z, Ma X, Kasik A, Li Z, Lin Y S. Gas separation properties of metal organic framework (MOF-5) membranes. *Industrial & Engineering Chemistry Research*, 2012, 52(3): 1102–1108
- Cohen-Tanugi D, Grossman J C. Water desalination across nanoporous graphene. *Nano Letters*, 2012, 12(7): 3602–3608
- Wang W, Eftekhari E, Zhu G, Zhang X, Yan Z, Li Q. Graphene oxide membranes with tunable permeability due to embedded carbon dots. *Chemical Communications*, 2014, 50(86): 13089–13092
- Kang J, Zhang H, Duan X, Sun H, Tan X, Liu S, Wang S. Magnetic Ni-Co alloy encapsulated N-doped carbon nanotubes for catalytic membrane degradation of emerging contaminants. *Chemical Engineering Journal*, 2019, 362: 251–261
- Shen J, Liu G, Huang K, Chu Z, Jin W, Xu N. Subnanometer two-dimensional graphene oxide channels for ultrafast gas sieving. *ACS Nano*, 2016, 10(3): 3398–3409
- Shahzad F, Alhabeb M, Hatter C B, Anasori B, Man Hong S, Koo C M, Gogotsi Y. Electromagnetic interference shielding with 2D transition metal carbides (MXenes). *Science*, 2016, 353(6304): 1137–1140
- Naguib M, Mashtalir O, Carle J, Presser V, Lu J, Hultman L, Gogotsi Y, Barsoum M W. Two-dimensional transition metal carbides. *ACS Nano*, 2012, 6(2): 1322–1331
- Wang H W, Naguib M, Page K, Wesolowski D J, Gogotsi Y. Resolving the structure of Ti₃C₂T_x MXenes through multilevel structural modeling of the atomic pair distribution function. *Chemistry of Materials*, 2015, 28(1): 349–359
- Fan Y, Wei L, Meng X, Zhang W, Yang N, Jin Y, Wang X, Zhao M,

- Liu S. An unprecedented high-temperature-tolerance 2D laminar MXene membrane for ultrafast hydrogen sieving. *Journal of Membrane Science*, 2019, 569: 117–123
27. Feng A, Yu Y, Jiang F, Wang Y, Mi L, Yu Y, Song L. Fabrication and thermal stability of NH_4HF_2 -etched Ti_3C_2 MXene. *Ceramics International*, 2017, 43(8): 6322–6328
28. Li J, Li X, Van der Bruggen B. MXene-based membrane for molecular separation. *Environmental Science. Nano*, 2020, 7(5): 1289–1304
29. Ren C E, Hatzell K B, Alhabeab M, Ling Z, Mahmoud K A, Gogotsi Y. Charge- and size-selective ion sieving through $\text{Ti}_3\text{C}_2\text{T}_x$ MXene membranes. *Journal of Physical Chemistry Letters*, 2015, 6(20): 4026–4031
30. Ding L, Wei Y, Wang Y, Chen H, Caro J, Wang H. A two-dimensional lamellar membrane: MXene nanosheet stacks. *Angewandte Chemie International Edition*, 2017, 56(7): 1825–1829
31. Ding L, Wei Y, Li L, Zhang T, Wang H, Xue J, Ding L X, Wang S, Caro J, Gogotsi Y. MXene molecular sieving membranes for highly efficient gas separation. *Nature Communications*, 2018, 9(1): 155–161
32. Li L, Zhang T, Duan Y, Wei Y, Dong C, Ding L, Qiao Z, Wang H. Selective gas diffusion in two-dimensional MXene lamellar membranes: insights from molecular dynamics simulations. *Journal of Materials Chemistry. A, Materials for Energy and Sustainability*, 2018, 6(25): 11734–11742
33. Shen J, Liu G, Ji Y, Liu Q, Cheng L, Guan K, Zhang M, Liu G, Xiong J, Yang J, Jin W. 2D MXene nanofilms with tunable gas transport channels. *Advanced Functional Materials*, 2018, 28(31): 1801511–1801523
34. Zhou F, Tien H N, Dong Q, Xu W L, Li H, Li S, Yu M. Ultrathin, ethylenediamine-functionalized graphene oxide membranes on hollow fibers for CO_2 capture. *Journal of Membrane Science*, 2019, 573: 184–191
35. Shen J, Liu G, Huang K, Jin W, Lee K R, Xu N. Membranes with fast and selective gas-transport channels of laminar graphene oxide for efficient CO_2 capture. *Angewandte Chemie International Edition*, 2015, 54(2): 578–582
36. Kang Z, Wang S, Fan L, Zhang M, Kang W, Pang J, Du X, Guo H, Wang R, Sun D. *In situ* generation of intercalated membranes for efficient gas separation. *Communications Chemistry*, 2018, 1(1): 3–10
37. Deng Y, Shang T, Wu Z, Tao Y, Luo C, Liang J, Han D, Lyu R, Qi C, Lv W, Kang F, Yang Q H. Fast gelation of $\text{Ti}_3\text{C}_2\text{T}_x$ MXene initiated by metal ions. *Advanced Materials*, 2019, 31(43): 1902432–1902438
38. Naguib M, Adams R A, Zhao Y, Zemlyanov D, Varma A, Nanda J, Pol V G. Electrochemical performance of MXenes as K-ion battery anodes. *Chemical Communications*, 2017, 53(51): 6883–6886
39. Xie Y, Dall’Agnese Y, Naguib M, Gogotsi Y, Barsoum M W, Zhuang H L, Kent P R. Prediction and characterization of MXene nanosheet anodes for non-lithium-ion batteries. *ACS Nano*, 2014, 8(9): 9606–9615
40. Tan X, Li K. Oxygen production using dense ceramic hollow fiber membrane modules with different operating modes. *AIChE Journal. American Institute of Chemical Engineers*, 2007, 53(4): 838–845
41. Wang H, Feldhoff A, Caro J, Schiestel T, Werth S. Oxygen selective ceramic hollow fiber membranes for partial oxidation of methane. *AIChE Journal. American Institute of Chemical Engineers*, 2009, 55(10): 2657–2664
42. Zhu J, Meng X, Zhao J, Jin Y, Yang N, Zhang S, Sunarso J, Liu S. Facile hydrogen/nitrogen separation through graphene oxide membranes supported on YSZ ceramic hollow fibers. *Journal of Membrane Science*, 2017, 535: 143–150
43. Alhabeab M, Maleski K, Anasori B, Lelyukh P, Clark L, Sin S, Gogotsi Y. Guidelines for synthesis and processing of two-dimensional titanium carbide ($\text{Ti}_3\text{C}_2\text{T}_x$ MXene). *Chemistry of Materials*, 2017, 29(18): 7633–7644
44. Ghidui M, Lukatskaya M R, Zhao M Q, Gogotsi Y, Barsoum M W. Conductive two-dimensional titanium carbide ‘clay’ with high volumetric capacitance. *Nature*, 2014, 516(7529): 78–81
45. Huang L, Li Y, Zhou Q, Yuan W, Shi G. Graphene oxide membranes with tunable semipermeability in organic solvents. *Advanced Materials*, 2015, 27(25): 3797–3802
46. Lukatskaya M R, Mashtalir O, Ren C E, Dall’Agnese Y, Rozier P, Taberna P L, Naguib M, Simon P, Barsoum M W, Gogotsi Y. Cation intercalation and high volumetric capacitance of two-dimensional titanium carbide. *Science*, 2013, 341(6153): 1502–1505
47. Ling Z, Ren C E, Zhao M Q, Yang J, Giammarco J M, Qiu J, Barsoum M W, Gogotsi Y. Flexible and conductive MXene films and nanocomposites with high capacitance. *Proceedings of the National Academy of Sciences of the United States of America*, 2014, 111(47): 16676–16681
48. Chi C, Wang X, Peng Y, Qian Y, Hu Z, Dong J, Zhao D. Facile preparation of graphene oxide membranes for gas separation. *Chemistry of Materials*, 2016, 28(9): 2921–2927
49. McKoy V, Sinanoğlu O. Theory of dissociation pressures of some gas hydrates. *Journal of Chemical Physics*, 1963, 38(12): 2946–2956
50. Kim H W, Yoon H W, Yoon S M, Yoo B M, Ahn B K, Cho Y H, Shin H J, Yang H, Paik U, Kwon S, Choi J Y, Park H B. Selective gas transport through few-layered graphene and graphene oxide membranes. *Science*, 2013, 342(6154): 91–95
51. Shamsaei E, Low Z X, Lin X, Mayahi A, Liu H, Zhang X, Zhe Liu J, Wang H. Rapid synthesis of ultrathin, defect-free ZIF-8 membranes via chemical vapour modification of a polymeric support. *Chemical Communications*, 2015, 51(57): 11474–11477
52. Li Y, Liang F, Bux H, Yang W, Caro J. Zeolitic imidazolate framework ZIF-7 based molecular sieve membrane for hydrogen separation. *Journal of Membrane Science*, 2010, 354(1-2): 48–54
53. Jia M, Feng Y, Liu S, Qiu J, Yao J. Graphene oxide gas separation membranes intercalated by UiO-66-NH_2 with enhanced hydrogen separation performance. *Journal of Membrane Science*, 2017, 539: 172–177
54. Hong Z, Sun F, Chen D, Zhang C, Gu X, Xu N. Improvement of hydrogen-separating performance by on-stream catalytic cracking of silane over hollow fiber MFI zeolite membrane. *International Journal of Hydrogen Energy*, 2013, 38(20): 8409–8414
55. Wang X, Chi C, Tao J, Peng Y, Ying S, Qian Y, Dong J, Hu Z, Gu Y, Zhao D. Improving the hydrogen selectivity of graphene oxide membranes by reducing non-selective pores with intergrown ZIF-8 crystals. *Chemical Communications*, 2016, 52(52): 8087–8090
56. Huang A, Liu Q, Wang N, Zhu Y, Caro J. Bicontinuous zeolitic

- imidazolate framework ZIF-8@GO membrane with enhanced hydrogen selectivity. *Journal of the American Chemical Society*, 2014, 136(42): 14686–14689
57. Elyassi B, Sahimi M, Tsotsis T T. Silicon carbide membranes for gas separation applications. *Journal of Membrane Science*, 2007, 288(1-2): 290–297
58. Xu G, Yao J, Wang K, He L, Webley P A, Chen C, Wang H. Preparation of ZIF-8 membranes supported on ceramic hollow fibers from a concentrated synthesis gel. *Journal of Membrane Science*, 2011, 385-386: 187–193
59. Liu Y, Peng Y, Wang N, Li Y, Pan J H, Yang W, Caro J. Significantly enhanced separation using ZIF-8 membranes by partial conversion of calcined layered double hydroxide precursors. *ChemSusChem*, 2015, 8(21): 3582–3586
60. Park H J, Suh M P. Enhanced isosteric heat, selectivity, and uptake capacity of CO₂ adsorption in a metal-organic framework by impregnated metal ions. *Chemical Science (Cambridge)*, 2013, 4(2): 685–690